

# Prediction of severe thunderstorm events with ensemble deep learning and radar data

Sabrina Guastavino<sup>a</sup>, Michele Piana<sup>a,1</sup>, Marco Tizzi<sup>c</sup>, Federico Cassola<sup>c</sup>,  
Antonio Iengo<sup>c</sup>, Davide Sacchetti<sup>c</sup>, Enrico Solazzo<sup>c</sup>, Federico Benvenuto<sup>a</sup>

<sup>a</sup>*The MIDA group, Dipartimento di Matematica, Università di Genova, Genova, Italy*

<sup>b</sup>*CNR - SPIN Genova, Genova, Italy*

<sup>c</sup>*ARPAL, Genova, Italy*

---

## Abstract

The problem of nowcasting extreme weather events can be addressed by applying either numerical methods for the solution of dynamic model equations or data-driven artificial intelligence algorithms. Within this latter framework, the present paper illustrates how a deep learning method, exploiting videos of radar reflectivity frames as input, can be used to realize a warning machine able to sound timely alarms of possible severe thunderstorm events. From a technical viewpoint, the computational core of this approach is the use of a value-weighted skill score for both transforming the probabilistic outcomes of the deep neural network into binary classification and assessing the forecasting performances. The warning machine has been validated against weather radar data recorded in the Liguria region, in Italy,

**Keywords:** weather forecasting; Doppler radar data; deep learning; convolutional neural networks; ensemble learning

**2010 MSC:** 68T07, 86A10

---

## 1. Introduction

One of the most interesting problems in weather forecasting is the prediction of extreme rainfall events such as severe thunderstorms possibly leading to flash floods. This problem is very challenging especially when we consider areas characterized by a complex, steep orography close to a coastline, where intense precipitation can be enhanced by specific topographic features: this is the case

---

*Email addresses:* guastavino@dima.unige.it (Sabrina Guastavino), piana@dima.unige.it (Michele Piana), marco.tizzi@arpal.liguria.it (Marco Tizzi), federico.cassola@arpal.liguria.it (Federico Cassola), antonio.iengo@arpal.liguria.it (Antonio Iengo), davide.sacchetti@arpal.liguria.it (Davide Sacchetti), enrico.solazzo@arpal.liguria.it (Enrico Solazzo), benvenuto@dima.unige.it (Federico Benvenuto)

for example of Liguria, an Italian region located on the North West Mediterranean Sea and characterized by the presence of mountains over 2000 m high at only few kilometres away from the coastline. This specific morphology gives rise to several catchments with steep slopes and limited extension [1]. Autumn events, when deep Atlantic troughs more easily enter the Mediterranean area and activate very moist and unstable flow lifted by the mountain range, may determine catastrophic flood on these coastal areas characterized by a high population density (see [2, 3] for a review of climatology and typical atmospheric configurations of extreme precipitations over the Mediterranean area). Just as an example, the November 4th 2011 flood in Genoa determined six deaths and economic damages up to 100 million euros [4, 5, 6, 7]). A common feature in these extreme events are the presence of a quasi-stationary convective system with a spatial extension of few kilometers [8, 9, 10, 11, 12]

Medium and long range either deterministic or ensemble Numerical Weather Prediction (NWP) models still struggle to correctly predict both the intensity and the location of these events, which can be triggered and enhanced by very small-scale features. High resolution convection-permitting NWP models manage to partly return a more realistic description of the dynamics of severe thunderstorms. Many studies addressed the role played by different components or settings of NWP models in order to better describe severe convective systems over the Liguria area, such as model resolution, initial conditions, microphysics schemes or small-scale patterns of the sea surface temperature ([6, 13, 14, 15, 16, 17, 18, 17, 19]).

However, the intrinsically limited predictability of convective systems requires the use of shorter-term *nowcasting* models, e.g. in order to feed automatic early warning systems, which may support meteorologists and hydrologist in providing accurate and reliable forecasts and thus preventing the consequences of these extreme events. These forecasting systems typically rely on two kinds of approaches. On the one hand, either stochastic or deterministic models are formulated utilizing partial differential equations in fluid dynamics, and numerical methods are implemented for their reduction, nesting hydrological models into meteorological ones [20, 21, 22]. On the other hand, more recent data-driven techniques take as input a time series of radar (and in case satellite) images belonging to a historical archive and provide as output a synthetic image representing the prediction of the radar signal at a subsequent time point; this approach can rely on some extrapolation technique, e.g. based on storm tracking systems [23] or on a diffusive process in Fourier space [24], or on deep learning networks [25, 26, 27, 28, 29, 30, 31, 32, 33, 34]. Mixed techniques have been also proposed blending NWP outputs with data-driven synthetic predictions [35].

The present study introduces a novel way to utilize deep learning for precipitation nowcasting using time series of radar images. Indeed, this approach provides probabilistic outcomes concerning the event occurrence and related quantitative parameters, thus realizing an actual warning machine for the forecasting of extreme events.

The main ingredients of this approach are three.

First, the design of the neural network combines a convolution neural network (CNN) with a Long Short-Term Memory (LSTM) network [36, 37] in order to construct a Long-term Recurrent Convolutional Network (LRCN) [38]. Second, for the first time in this kind of forecasting problems, the prediction assessment is realized by means of value-weighted skill scores that account for the distribution of prediction along time [39], thus promoting prediction in advance. Finally, the third ingredient is concerned with the way the probabilistic outcomes of the network are transformed into binary classification. Inspired by [39], we use an ensemble learning technique that realizes an automatic choice of the level with which epochs have to be involved in the definition of prediction.

The results of this study show that the use of a value-weighted skill score in the framework of an ensemble approach allows the deep network to provide predictions more accurate than those obtained when standard quality-based skill scores are applied.

The paper is organized as follows. In Section 2 we describe the considered weather radar and lightning data and in Section 3 we give details on the architecture of the LRCN model used in this study. In Section 4 we recall the definition of value-weighted skill scores and we describe the proposed ensemble deep learning technique. In Section 5 we show the effectiveness of the method in prediction of extreme rainfall events using radar-based data. Our conclusions are offered in section 6.

## 2. Constant Altitude Plan Position Indicator reflectivity data in Liguria

Precipitation activity and locations of rain, showers, and thunderstorms are commonly monitored in real-time by polarimetric Doppler weather radars; return echoes from targets (such as hydrometeors) allow the measurement of the reflectivity field on different conic surfaces at each radar elevation; however, reflectivity values at a certain height can be interpolated to 2D maps, which are also known as Constant Altitude Plan Position Indicator (CAPPI) images [40]; such a representation is particularly useful in order to compose reflectivity data measured by different radars over overlapping regions, returning a reflectivity field for the larger area covered by a radar network.

In our study CAPPI reflectivity fields measured by the Italian Radar Network within the Civil Protection Department are considered. CAPPI images, measured in dbZ, are sampled every 10 minutes at a spatial resolution of  $0.005^\circ \simeq 0.56$  km in latitude and  $0.005^\circ \simeq 0.38$  km in longitude. We used CAPPI images at three different heights (2 km, 3 km, and 5 km a.s.l.) and cut each image over an area comprising the Liguria region (as shown in Figure 1). In detail, for each image the latitude ranges in  $[43.4^\circ \text{ N}, 45.0^\circ \text{ N}]$  and the longitude ranges in  $[7.1^\circ \text{ E}, 10.4^\circ \text{ E}]$ , so that images have size  $321 \times 661$  and cover an area of about 180 km in latitude and 250 km in longitude. We used 1 hour and a half long movies of CAPPI images to construct temporal features sequences to predict the occurrence of extreme rainfall event in the next hour from the last frame time of the radar movie.

The training set exploited to optimize the CNN is generated by means of a labeling procedure involving Modified Conditional Merging (MCM) data and lightning data. MCM data [41] combine radar rain estimates and rain gauges measurements with a hourly frequency and provide the amount of rain fallen on ground integrated over 1 hour (in these data the content of each pixel is measured in mm per hour and the spatial resolution is  $0.013267^\circ \simeq 1$  km in longitude and  $0.008929^\circ \simeq 1$  km in latitude; see Figure 1). Lightning data are recorded by the LAMPINET network of Military Aeronautics [42] and have a resolution of 1 microsecond.

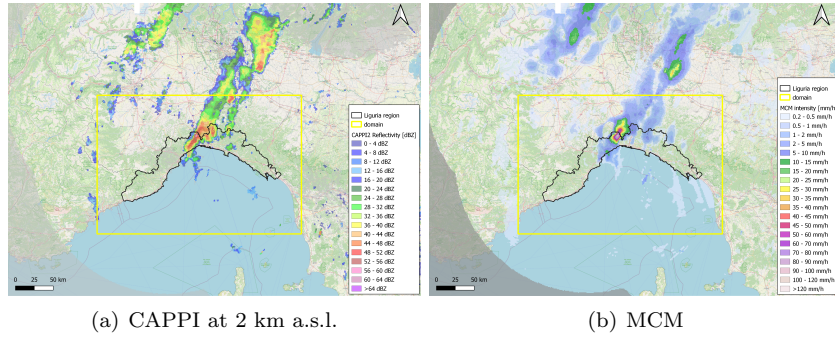


Figure 1: An example of a 2-km CAPPI reflectivity frame (left) and a MCM rain rate frame (right) (both referred to 21/10/2019 23:00 UTC); the selected area surrounding Liguria region is delimited in yellow.

The labeling process associates each CAPPI video to the concept of severe convective rainfall event, whose definition relies on the following two items:

- MCM data must contain at least 3 contiguous pixels exceeding 50 mm/h within the selected area;
- at least 10 lightnings must consecutively occur in a 10 minutes time range in the area comprising 5 km around each one of the MCM pixel with over-threshold content.

It is worth noticing that 50 mm/h is regarded as a threshold for heavy rain in the Liguria region; however, the first condition accounts for the fact that an over-threshold value associated to an isolated pixel may be associated to spurious non-meteorological echoes like, for instance, the passage of a plane. On the other hand, the second condition implies that the extreme events considered must always involve the occurrence of thunderstorms.

### 3. Long-term Recurrent Convolutional Network

Long-term Recurrent Convolutional Networks (LRCNs) [43] combine a Convolutional Neural Network (CNN) and a Long Short-Term Memory (LSTM)



network to create spatio-temporal deep learning models. In this application, the input is made of time series of 10 radar reflectivity images (representing a video of one hour and half radar images) at the three CAPPI 2, CAPPI 3 and CAPPI 5 levels, which refer to 2 km, 3 km and 5 km a.s.l., respectively. The CNN is used to automatically extract signal features from the image set. The features are decomposed into sequential components and fed to the LSTM network to be analyzed. Finally, the output of the LSTM layer is fed into the fully connected layer and the sigmoid activation function is applied to generate the probability distribution of the positive class. Figure 2 shows the architecture of the LRCN model.

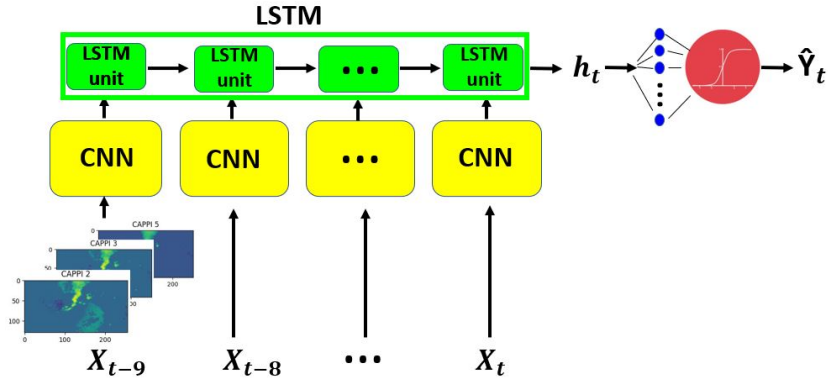


Figure 2: The LRCN architecture.

### 3.1. The CNN architecture

The CNN architecture of the LRCN model consists in three blocks, each one composed by a convolutional layer with stride (2, 2), followed by a batch normalization layer to improve stability; the Rectified Linear Unit (ReLU) function [44] is adopted as an activation function and the max pooling operation with size (4, 4) and stride (2, 2) is applied. We initialize all the convolutional weights by sampling from the scaled uniform distribution [45]. The three convolutional layers are characterized by 8, 16 and 32 kernels with size (5, 5), (3, 3) and (3, 3), respectively. The input are sequences of size  $(T, 128, 256, 3)$ , where  $T$  represents the number of frames in each movie, 128 and 256 correspond to the image size (in pixel) and 3 represents the three levels of CAPPI data. In all operations we take advantage of the “Timedistributed” layer, available in the Keras library [46], which allows the in parallel training of the  $T$  convolutional flows. Figure 3 illustrates this CNN architecture.

**Remark 1.** *The choice of the kernel size is driven by the idea of capturing features in a larger neighborhood of the first layer, where the size is equal to (5, 5); the size is decreased to (3, 3) in the last two layers. As it is shown in [25], smaller kernel sizes are suggested in this problem since kernels with larger size*

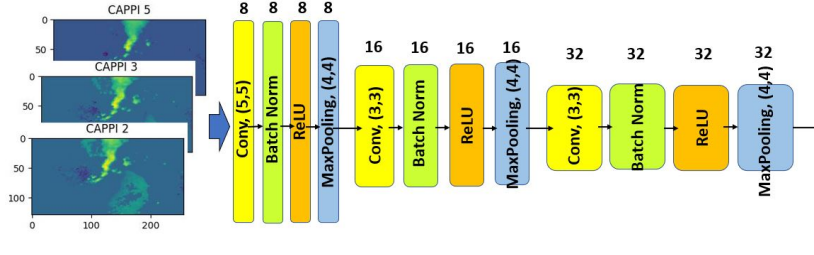


Figure 3: The CNN architecture.

lead to overfitting and to more uncertain predictions. The number of kernels is a trade off between the amount of number of parameters and the obtained performances. We tested the network performances for a decreasing number of kernels in the second and third layer while keeping the number of kernels in the first layer fixed. This led to more and more overfitting, and higher and higher uncertainty of predictions. On the other hand, the CNN is rather robust while increasing the number of kernels in the first and second layers without changing the number of kernels in the third layer.

### 3.2. Long Short-Term Memory

The CNN output is flattened to create the sequence of feature vectors to feed into the LSTM network. LSTM is a particular form of recurrent neural network (RNN), which is the general term used to name a set of neural networks able to process sequential data. The LSTM unit is characterized by three “gate” structures: “input”, “forget” and “output” gates. At every timestep  $t$ , the input  $x_t$ , i.e. the  $t$ -th element of the input sequence, and the output  $h_{t-1}$  of the memory cells at the previous timestep  $t - 1$  are presented to the three gates, which have the purpose of filtering the information as follows:

- The “forget” gate defines which information is removed from the cell state.
- The “input” gate specifies which information is added to the cell state.
- The “output” gate specifies which information from the cell state is used as output.

We consider the following notations:

- $x_t$  is the input vector at timestep  $t$ ;
- $W_{xf}, W_{hf}, W_{cf}, W_{xi}, W_{hi}, W_{ci}, W_{xo}, W_{ho}, W_{co}$  are the weight matrices;
- $b_f, b_i, b_o$  are the bias vectors;
- $f_t, i_t, o_t$  are the vectors for the activation values of the respective gates;
- $c_t$  and  $c_{t-1}$  are the cell state at timesteps  $t$  and  $t - 1$ , respectively;

- $h_t$  is the output vector of the LSTM layer.

The LSTM procedure is described by the following equations:

$$i_t = \sigma(W_{xi}x_t + (W_{hi}h_{t-1} + W_{ci} \circ c_{t-1} + b_i)); \quad (1)$$

$$f_t = \sigma(W_{xf}x_t + W_{hf}h_{t-1} + W_{cf} \circ c_{t-1} + b_f); \quad (2)$$

$$c_t = f_t \circ c_{t-1} + i_t \circ \tanh(W_{xc}x_t + W_{hc}h_{t-1} + b_c); \quad (3)$$

$$o_t = \sigma(W_{xo}x_t + W_{ho}h_{t-1} + W_{co} \circ c_t + b_o); \quad (4)$$

$$h_t = o_t \circ \tanh(c_t), \quad (5)$$

where  $\circ$  denotes the Hadamard product and  $\sigma$  is the sigmoid function. Therefore, the input information will be accumulated to the cell if the “input” gate  $i_t$  is activated. Also, the past cell status  $c_{t-1}$  could be “forgotten” in this process if the “forget” gate  $f_t$  is on. If the latest cell output  $c_t$  will be propagated to the final state,  $h_t$  is further controlled by the “output” gate  $o_t$ . A representation of an LSTM unit is shown in Figure 4.

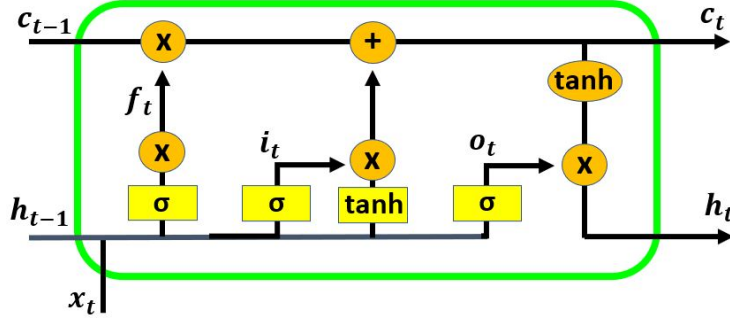


Figure 4: LSTM unit.

In our experiments, the LSTM layer has 50 hidden neurons. Finally, the dropout layer is used to prevent overfitting [47]: the dropout value is set to 0.5, meaning that 50% of neurons are randomly dropped from the neural network during training in each iteration.

### 3.3. Loss function

Once the architecture of the NN is set up, we can denote with  $\theta$  the NN weights and we can interpret the NN as a map  $f_\theta$ , mapping a sample  $X$  to a probability outcome  $f_\theta(X) \in [0, 1]$ , since the sigmoid activation function is applied in the last layer. We recall that, in our application, the sample  $X$  is a video of CAPPI reflectivity images and  $f_\theta(X)$  represents the predicted probability of the occurrence of an extreme rainfall event in the next hour after the end time of the CAPPI video  $X$  within the selected area (in fact, we are not interested in the exact location of the possible event). In the training process we consider a minimization problem

$$\min_{\theta} \ell(F_\theta(\mathbf{X}), \mathbf{Y}), \quad (6)$$

where  $\{\mathbf{X}, \mathbf{Y}\} = \{(X_i, Y_i)\}_{i=1}^n$  is the training set ( $Y_i$  represents the actual label of the sample  $X_i$  according to the definition given in section 2),  $F_\theta(\mathbf{X}) = (f_\theta(X_i))_i$  represents the probability outcomes of the NN on the set  $\mathbf{X}$  and  $\ell$  represents the loss function measuring the discrepancy between the true label  $\mathbf{Y}$  and the predicted output  $F_\theta(\mathbf{X})$ . In classification problems the most used loss function is the binary cross-entropy or (categorical cross-entropy if labels are one-hot encoded). In the case of imbalanced data sets, modifications of the cross-entropy loss are considered, such as the following one:

$$\ell(f_\theta(\mathbf{X}), \mathbf{Y}) = - \left( \sum_{i=1}^n \beta_1 Y_i \log(f_\theta(X_i)) + \beta_0 (1 - Y_i) \log(1 - f_\theta(X_i)) \right), \quad (7)$$

where  $\beta_0, \beta_1$  are positive weights defined according to the data set imbalance. We define the weights as

$$\beta_1 = \frac{1}{\#\{i \in \{1, \dots, n\} : Y_i = 1\}} \text{ and } \beta_0 = \frac{1}{\#\{i \in \{1, \dots, n\} : Y_i = 0\}}, \quad (8)$$

and we refer to the chosen loss function as the class balanced cross-entropy.

#### 4. Ensemble deep learning

Ensemble deep learning is made of two ingredients: a criterion for assessing the prediction accuracy and a strategy for transforming a probabilistic outcome into a binary classification.

##### 4.1. Evaluation skill scores

The result of a binary classifier is usually evaluated by computing the confusion matrix, also known as contingency table. Let us denote with  $\mathbb{M}_{2,2}(\mathbb{N})$  the set of 2-dimensional matrices with natural elements. Let  $\mathbf{Y} = (Y_i) \in \{0, 1\}^n$  be a binary sequence representing the actual labels of a given dataset of examples, and let  $\hat{\mathbf{Y}} = (\hat{Y}_i) \in \{0, 1\}^n$  be a binary sequence representing the prediction. Then the classical (quality-based) confusion matrix  $\mathbf{C} \in \mathbb{M}_{2,2}(\mathbb{N})$  is given by:

$$\tilde{\mathbf{C}}(\hat{\mathbf{Y}}, \mathbf{Y}) = \begin{pmatrix} \text{TN} & \text{FP} \\ \text{FN} & \text{TP} \end{pmatrix},$$

where

- $\text{TP} = \sum_{i=1}^n \mathbb{1}_{\{Y_i=1, \hat{Y}_i=1\}}$  represents the True Positives, i.e. the number of samples correctly classified as positive class;
- $\text{TN} = \sum_{i=1}^n \mathbb{1}_{\{Y_i=0, \hat{Y}_i=0\}}$  represents the True Negatives, i.e. the number of samples correctly classified as negative class;
- $\text{FP} = \sum_{i=1}^n \mathbb{1}_{\{Y_i=0, \hat{Y}_i=1\}}$  represents the False Positives, i.e. the number of negative samples incorrectly classified as positive class;

- $\text{FN} = \sum_{i=1}^n \mathbb{1}_{\{Y_i=1, \hat{Y}_i=0\}}$  represents the False Negatives, i.e. the number of positive samples incorrectly classified as negative class.

A specific classical (quality-based) skill score is given by a map  $S : \mathbb{M}_{2,2}(\mathbb{N}) \rightarrow \mathbb{R}$  defined on the confusion matrix  $\tilde{\mathbf{C}}$ . In this study we considered two skill-scores, i.e., the Critical Success Index (CSI)

$$\text{CSI}(\tilde{\mathbf{C}}(\hat{\mathbf{Y}}, \mathbf{Y})) = \frac{\text{TP}}{\text{TP} + \text{FP} + \text{FN}}, \quad (9)$$

which is commonly used in meteorological applications [34]; and the True Skill Statistic (TSS)

$$\text{TSS}(\tilde{\mathbf{C}}(\hat{\mathbf{Y}}, \mathbf{Y})) = \frac{\text{TP}}{\text{TP} + \text{FN}} - \frac{\text{FP}}{\text{FP} + \text{TN}}, \quad (10)$$

which is particularly appropriate for imbalanced data sets [48]. CSI assumes values in  $[0, 1]$ , while TSS assumes values in  $[-1, 1]$  and for both scores the optimal value is 1.

However, such metrics do not account for the distribution of predictions along time and are not able to provide a quantitative preference to those alarms that predict an event in advance with respect to its actual occurrence, and to penalize predictions sounding delayed false alarms. In order to overtake such limitation, value-weighted confusion matrices have been introduced [39]. In fact, a value-weighted confusion matrix is defined as

$$\mathbf{C}_w(\hat{\mathbf{Y}}, \mathbf{Y}) = \begin{pmatrix} \text{TN} & \text{wFP} \\ \text{wFN} & \text{TP} \end{pmatrix}, \quad (11)$$

with

$$\text{wFP} = \sum_{i=1}^n w(z_i^-, z_i^+) \mathbb{1}_{\{Y_i=0, \hat{Y}_i=1\}}, \quad (12)$$

$$\text{wFN} = \sum_{i=1}^n w(\hat{z}_i^+, \hat{z}_i^-) \mathbb{1}_{\{Y_i=1, \hat{Y}_i=0\}}. \quad (13)$$

The weights  $w(z_i^-, z_i^+)$  and  $w(z_i^-, z_i^+)$  are constructed as follows. Given the label  $Y_i$  observed at the sampled time  $i$ , then

$$z_i^- = (Y_{i-1}, Y_{i-2}, \dots, Y_{i-T}), \quad (14)$$

is the sequence of the  $T$  elements before  $Y_i$  and

$$z_i^+ = (Y_{i+1}, Y_{i+2}, \dots, Y_{i+T}) \quad (15)$$

is the sequence of the  $T$  elements after  $Y_i$ . Analogously, given the label  $\hat{Y}_i$  predicted at time  $i$ , then

$$\hat{z}_i^- = (\hat{Y}_{i-1}, \hat{Y}_{i-2}, \dots, \hat{Y}_{i-T}), \quad (16)$$

and

$$\hat{z}_i^+ = (\hat{Y}_{i+1}, \hat{Y}_{i+2}, \dots, \hat{Y}_{i+T}). \quad (17)$$

The weight function  $w : \mathbb{R}^T \times \mathbb{R}^T \rightarrow \mathbb{R}$  is constructed in such a way to emphasize

- false positives associated to alarms predicted in the middle of  $2T + 1$ -long time windows when no actual event occurs; and
- false negatives associated to missed events in the middle of  $2T + 1$ -long time windows in which no alarm is raised.

We wanted to mitigate as well false positives that anticipate the occurrence of events and false negatives which are preceded by predicted alarms. An example for a possible shape of this function is given in [39], in which the function  $w$  is defined as follows;

$$w(s, t) = \begin{cases} 2 & \text{if } s, t \equiv 0 \\ 1 - \max(w \circ t) & \text{otherwise} \end{cases} \quad (18)$$

where  $w := \left(\frac{1}{2}, \frac{1}{3}, \dots, \frac{1}{T+1}\right)$  and  $w \circ t$  indicates the element-wise product.

The introduction of this value-weighted confusion matrix allows the construction of the associated value-weighted Critical Success Index wCSI and the value-weighted True Skill Statistic wTSS, respectively.

#### 4.2. Ensemble strategy

We consider an ensemble procedure to provide an automatic classifier from the probability outcomes provided by the deep NN. This procedure has been introduced in [39], and it can be summarized in the following steps:

1. Consider the first  $N$  epochs of the training process of the deep neural network  $f_\theta$ . Define  $\theta_j := \theta_j(\{\mathbf{X}, \mathbf{Y}\})$  the weights for each epoch  $j$ .
2. Select the classification threshold. Let  $\tau$  be a threshold; we define the binary point-wise prediction at epoch  $j$  with respect to the threshold  $\tau$  as

$$p_{\theta_j}^\tau(\cdot) := \mathbf{1}_{\{f_{\theta_j}(\cdot) > \tau\}} \quad (19)$$

and we denote with

$$P_{\theta_j}^\tau(\mathbf{X}) := (p_{\theta_j}^\tau(X_i))_i \quad (20)$$

the binary prediction on the set of samples  $\mathbf{X}$ . For each epoch  $j$  choose the real number that maximizes a given skill scores  $S$ , i.e.

$$\bar{\tau}_j = \arg \max_{\tau \in [0,1]} S(\mathbf{C}(P_{\theta_j}^\tau(\mathbf{X}), \mathbf{Y})). \quad (21)$$

We denote with

$$\bar{p}_{\theta_j}(\cdot) := p_{\theta_j}^{\bar{\tau}_j}(\cdot) \quad (22)$$

the binary prediction with respect to the selected optimal threshold  $\bar{\tau}_j$  and consequently with

$$\bar{P}_{\theta_j}(\mathbf{X}) = (\bar{p}_{\theta_j}(X_i))_i, \quad (23)$$

the binary prediction on the set  $\mathbf{X}$ .

3. Consider a validation set  $\{\tilde{\mathbf{X}}, \tilde{\mathbf{Y}}\} = \{(\tilde{X}_i, \tilde{Y}_i)\}_{i=1}^m$ . Given a quality level  $\alpha$ , select the epochs for which the skill score  $S$  computed on the validation set is higher than  $\alpha$ . This allows the selection of the set of epochs

$$\mathcal{J}_\alpha := \{j \in \{1, \dots, N\} : S(\mathbf{C}(\bar{P}_{\theta_j}(\tilde{\mathbf{X}}), \tilde{\mathbf{Y}})) > \alpha\}. \quad (24)$$

4. Define the ensemble prediction as the binary value corresponding to the median value  $m$  among all binary predictions associated to  $\mathcal{J}_\alpha$ , i.e. given a new sample  $X$  the output is defined as

$$\hat{Y}^\theta = m(\{\bar{p}_{\theta_j}(X) : j \in \mathcal{J}_\alpha\}). \quad (25)$$

In the case where the number of zeros is equal to the number of ones, we assume  $\hat{Y}^\theta = 1$ .

In the previous scheme the parameter  $\alpha$  in equation (24) can be fixed according to the following procedure:

1. For each  $\gamma \in [\gamma_0, \gamma_1]$  with  $0 < \gamma_0 < \gamma_1 < 1$ :
  - (a) Define  $\alpha_\gamma := \gamma \max_{j \in \{1, \dots, N\}} (S(\mathbf{C}(\bar{p}_{\theta_j}(\tilde{\mathbf{X}}), \tilde{\mathbf{Y}})))$ , which represents a fraction of the maximum score  $S$  obtained on the validation set by varying epochs.
  - (b) Select the epochs for which the skill score  $S$  computed on the validation set is higher than  $\alpha_\gamma$

$$\mathcal{J}_{\alpha_\gamma} := \{j \in \{1, \dots, N\} : S(\mathbf{C}(\bar{p}_{\theta_j}(\tilde{\mathbf{X}}), \tilde{\mathbf{Y}})) > \alpha_\gamma\}. \quad (26)$$

- (c) Compute the ensemble prediction on the validation set as follows

$$\hat{\mathbf{Y}}_\gamma^\theta = m(\{\bar{p}_{\theta_j}(\tilde{\mathbf{X}}) : j \in \mathcal{J}_{\alpha_\gamma}\}). \quad (27)$$

2. Select the optimal parameter  $\bar{\gamma}$  as the one which maximizes the skill score  $S$  computed between the validation labels and the ensemble prediction  $\hat{\mathbf{Y}}_\gamma^\theta$

$$\bar{\gamma} := \arg \max_{\gamma \in [\gamma_0, \gamma_1]} S(\mathbf{C}(\hat{\mathbf{Y}}_\gamma^\theta, \tilde{\mathbf{Y}})) \quad (28)$$

3. Define the optimal level as follows

$$\bar{\alpha} := \bar{\gamma} \max_{j \in \{1, \dots, N\}} (S(\mathbf{C}(\bar{P}_{\theta_j}(\tilde{\mathbf{X}}), \tilde{\mathbf{Y}}))). \quad (29)$$

This procedure allows an automatic choice of the level  $\alpha$  which depends on the validation results. In order to preserve statistical robustness, we propose to repeat the procedure  $M$  times, i.e. to train the deep NN  $M$  times (each time

the training set is fixed but the weights are randomly initialized) and take the ensemble prediction with the highest preferred skill score  $S'$  (which could be also different from  $S$ ) on the validation set. Summing up, by denoting with  $\theta^{(k)}$  the weights of the trained deep neural network at the  $k$ -th time, we define the optimal weights as

$$\bar{\theta} := \arg \max_{k=1, \dots, M} S'(\mathbf{C}(\hat{\mathbf{Y}}_{\bar{\gamma}}^{\theta^{(k)}}, \tilde{\mathbf{Y}})), \quad (30)$$

where  $\hat{\mathbf{Y}}_{\bar{\gamma}}^{\theta^{(k)}}$  is the ensemble prediction on the validation set obtained at the  $k$ -th time of the training process. In the following we show performances of the ensemble deep learning technique when the LRCN network is used for the problem of forecasting extreme rainfall events in Liguria.

## 5. Experimental results

In order to assess the prediction reliability of our deep NN model, we considered a historical dataset of CAPPI composite reflectivity videos recorded by the Italian weather Radar Network in the time window ranging from 2018/07/09 at 21:30 UTC to 2019/12/31 at 12:00 UTC, each video being 90 minutes long. For the training phase, we considered the time range from 2018/07/09 at 21:30 UTC to 2019/07/16 at 10:30 UTC and label the videos with binary labels concerning the concurrent occurrence of an over-threshold rainfall event from MCM data and lightning strikes in its surroundings, as explained in Section 2 (the training set contains 7128 samples overall, with 105 samples labeled with 1, i.e. corresponding to extreme events according to the definition given in Section 2). For the validation step, we considered the videos in the time range from 2019/07/19 at 14:30 UTC to 2019/09/30 at 12:30 UTC (the validation set is made of 1296 videos overall, with 48 videos labeled with 1). Eventually, the test set is made of the CAPPI videos in the time range between 2019/10/03 at 15:00 UTC and 2019/12/31 at 12:00 UTC (the test contains 1899 videos and 33 of them are labeled with 1). The model is trained over  $N = 100$  epochs using the Adam Optimizer [49] with learning rate equal to 0.001 and mini-batch size equal to 72. The class balanced cross-entropy defined in (7) is used as loss function in the training phase, where the weights  $\beta_0$  and  $\beta_1$  are defined as the inverse of the number of samples labeled with 0 and with 1 in each mini-batch, respectively,

As explained in Section 4, the statistical significance of the results is guaranteed by running the network  $M = 10$  times, each time with a different random initialization of the LRCN weights. Finally, we applied the ensemble strategy as described in Section 4, using the TSS and wTSS for choosing the epochs with best performances, respectively. For sake of clarity, for now on the two ensemble strategies will be named as TSS-ensemble and wTSS-ensemble, respectively.

These two strategies have been applied to the test set and the results are illustrated in Table 1, where we reported the average values and the corresponding standard deviations for the entries of the quality- and value-weighted confusion matrices, and for the TSS, CSI, wTSS, and wCSI. The table shows



Table 1: Results on the test set obtained by using the TSS-ensemble and wTSS-ensemble strategies. The entries are the average values of the scores over 10 runs of the network for 10 random initializations of the weights. The standard deviations are also included.

Strategy	Confusion matrix		TSS	CSI	wFP	wFN	wTSS	wCSI
wTSS	TN = 1725.40( $\pm 21.98$ ) FN = 4.70( $\pm 1.25$ )	FP = 140.60( $\pm 21.98$ ) TP = 28.30( $\pm 1.25$ )	0.78( $\pm 0.04$ )	0.17( $\pm 0.02$ )	243.88( $\pm 41.34$ )	6.79( $\pm 1.64$ )	0.68( $\pm 0.04$ )	0.10( $\pm 0.02$ )
TSS	TN = 1727.60( $\pm 32.42$ ) FN = 5.10( $\pm 1.85$ )	FP = 138.40( $\pm 32.42$ ) TP = 27.90( $\pm 1.85$ )	0.77( $\pm 0.05$ )	0.17( $\pm 0.03$ )	240.99( $\pm 60.57$ )	7.24( $\pm 2.60$ )	0.67( $\pm 0.06$ )	0.10( $\pm 0.02$ )

Table 2: Results on the test set obtained by using the wTSS-ensemble strategy when the run is selected with respect to the best TSS or wTSS ( $k = 7$  run), the wTSS-ensemble strategy when the run is selected with respect to the best CSI or wCSI ( $k = 9$  run) and the TSS-ensemble strategy when the run is selected with respect to the best TSS or wTSS or CSI or wCSI ( $k = 10$  run). In bold the best results are highlighted.

Score	Strategy			
	wTSS ensemble		TSS ensemble	
	$S' = \text{TSS/wTSS (run } k = 7)$	$S' = \text{CSI/wCSI (run } k = 9)$	$S' = \text{TSS/wTSS/CSI/wCSI (run } k = 10)$	
Confusion matrix	TN = 1730 FN = <b>4</b>	FP = 136 TP = <b>29</b>	TN = 1765 FN = <b>4</b>	FP = 101 TP = <b>29</b>
TSS	0.8059	<b>0.8247</b>	0.7651	
CSI	0.1716	<b>0.2164</b>	0.2045	
wFN	<b>4.75</b>	8	8	
wFP	229.83	<b>166.58</b>	171.67	
wTSS	<b>0.742</b>	0.6975	<b>0.6829</b>	
wCSI	0.11	<b>0.1425</b>	0.1306	

that the score values are all rather similar, although the averaged TSS and wTSS values are slightly higher when the wTSS-ensemble strategy is adopted. Since, according to the ensemble strategy, the prediction for a specific test set is made by using the weights corresponding to the best run in the validation set, in Figure 5 we show the behavior of TSS and wTSS for the TSS-ensemble and wTSS-ensemble strategies, in the case of 10 runs of the network corresponding to 10 random initializations of the weights.

The results in this Figure imply that, in the case of the wTSS-ensemble strategy, the best score values in validation correspond to the best score values in the test phase. Figure 6 illustrates the same analysis in the case when the scores used for assessing the prediction performances are CSI and wCSI and shows that, also in this case, the wTSS-ensemble strategy should be preferred.

Table 2 contains the values of the entries of the confusion matrices and of the scores obtained by using the weights associated to the best runs of the network selected during the validation phase by means of the TSS-ensemble and wTSS-ensemble strategies. Please consider that in the case of the TSS-ensemble strategy the best run is always the  $k = 10$  one.

In order to show how the use of value-weighted scores perform in action, in Figure 7 we enrolled over time the predictions corresponding to the test set, when the wTSS-ensemble and TSS-ensemble strategies are adopted and when wTSS, TSS, wCSI and CSI are used for selecting the best run (we point out again that using wTSS and TSS for the wTSS-ensemble strategy always leads to  $k = 7$  and that using wCSI and CSI for the same ensemble strategy always leads to  $k = 9$ ). We remind that the labeling procedure depends on the rain rate and on the presence of lighting as described in Section 2: the blue bars

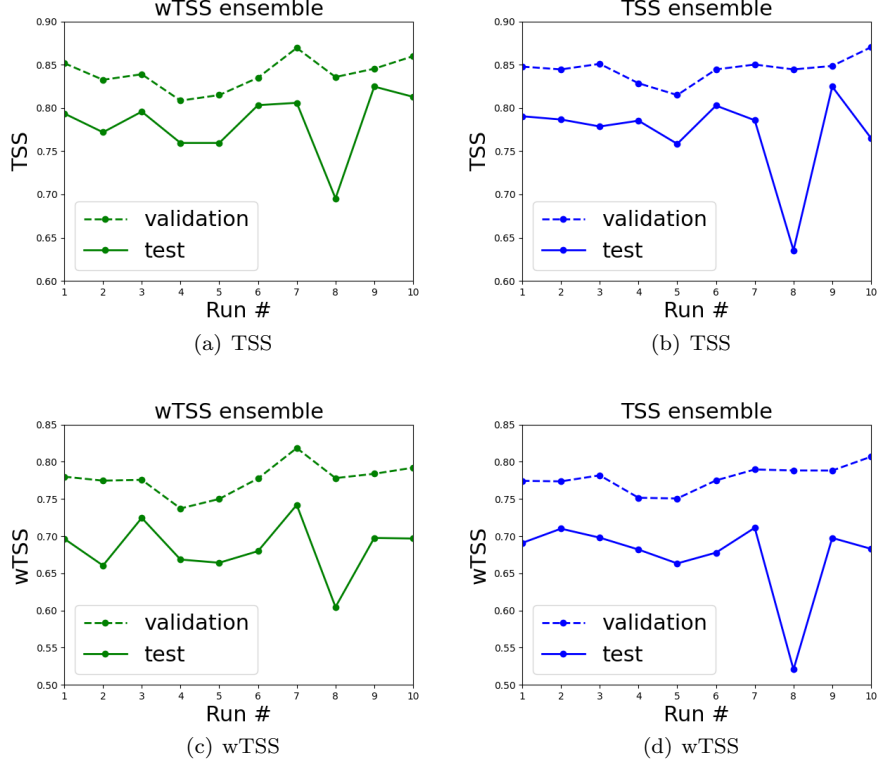


Figure 5: First row: the TSS values on validation set (dashed lines) and test set (continuous lines) obtained on each run by applying the wTSS-ensemble strategy (left panel) and the TSS-ensemble strategy (right panel). Second row: the wTSS values on validation set (dashed lines) and test set (continuous lines) obtained on each run by applying the wTSS-ensemble strategy (left panel) and the TSS-ensemble strategy (right panel).

represent the events labeled with 1, i.e. events which satisfy the condition on both the rain rate and the presence of lighting, whereas the green bars are events that satisfy just only the condition on the rain rate. We first point out that when the wTSS-strategy is used and  $k = 7$  is selected, the prediction tends to systematically anticipate the events characterized by high rain rate. Further, for sake of clarity, Figure 8 contains a zoom around the November 22 2019 time point, when a dramatic flood caused significant damages in many areas of Liguria. This zoom shows that the wTSS-ensemble strategy for  $k = 7$  is able to correctly predict the thunderstorms occurring in the time interval from 00:00 to 02:00 UTC and to anticipate the other catastrophic thunderstorm occurring between 10:00 and 11:00 UTC (this last thunderstorm is marked with a blue arrow in all panels of Figure 8). No anticipated alarm is sounded by the other two predictions.

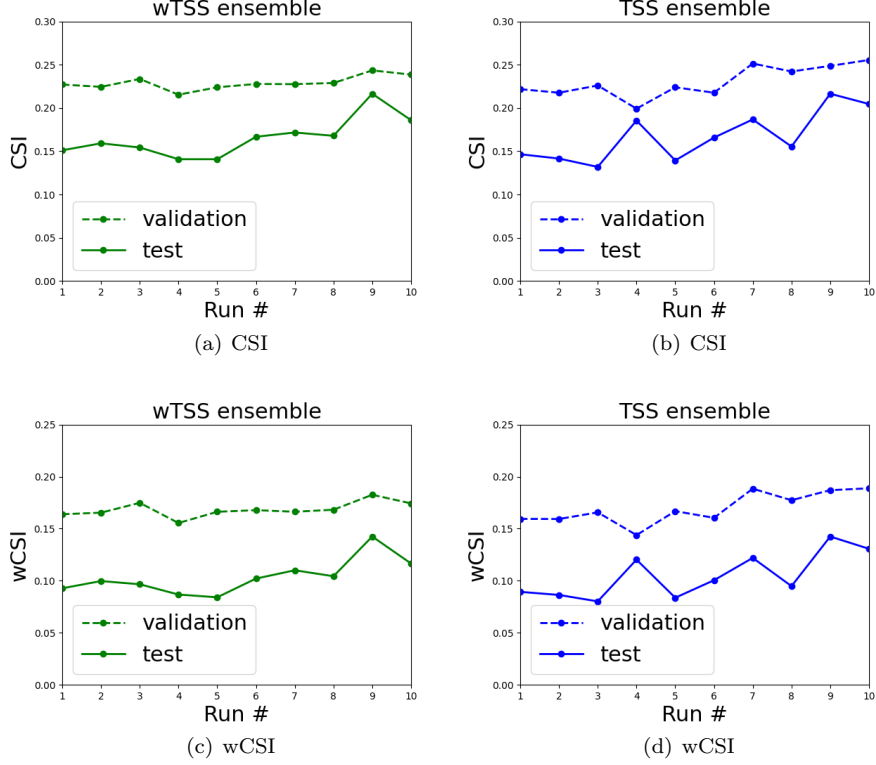
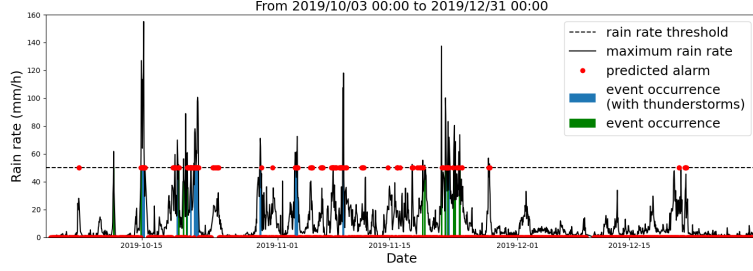


Figure 6: First row: the CSI values on validation set (dashed lines) and test set (continuous lines) obtained on each run by applying the wTSS-ensemble strategy (left panel) and the TSS-ensemble strategy (right panel). Second row: the wCSI values on validation set (dashed lines) and test set (continuous lines) obtained on each run by applying the wTSS-ensemble strategy (left panel) and the TSS-ensemble strategy (right panel).

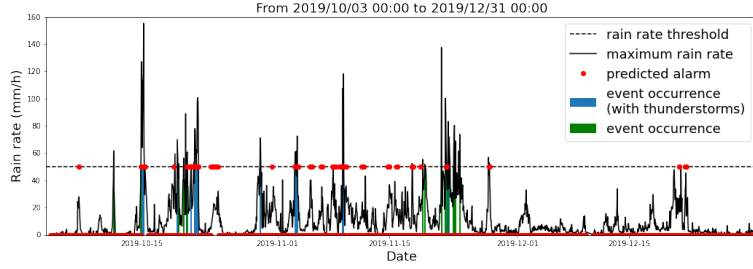
## 6. Conclusions

The realization of warning machines able to sound binary alarms along time is an intriguing issue in many areas of forecasting [50, 51, 52, 53]. The present paper shows for the first time that a deep CNN exploiting radar videos as input can be used as a warning machine for predicting severe thunderstorms (in fact, previous CNNs in this field have been used to synthesize simulated radar images at time points successive to the last one in the input time series). It is worth noticing that the aim here is not the prediction of the exact location and intensity of a heavy rain event, but rather the probable occurrence of a severe thunderstorm over a reference area in the next hour.

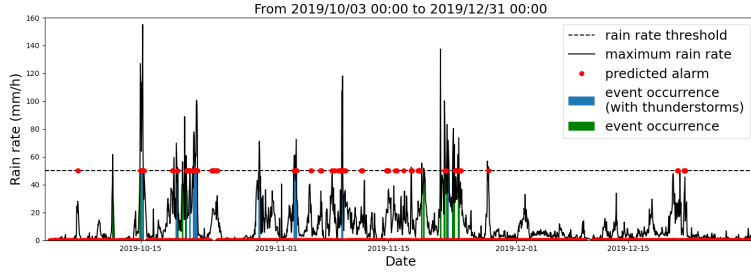
The crucial point in our approach relies on the kind of evaluation metrics adopted. In fact, the TSS can be considered a good measure of performances in forecasting, since it is insensitive to the class-imbalance ratio. However, such



(a) wTSS-ensemble ( $k = 7$ )



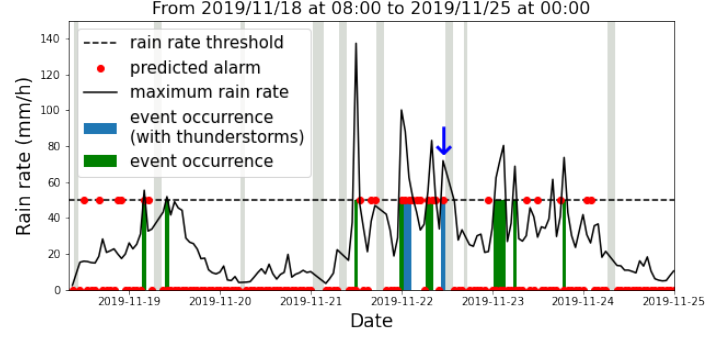
(b) wTSS-ensemble ( $k = 9$ )



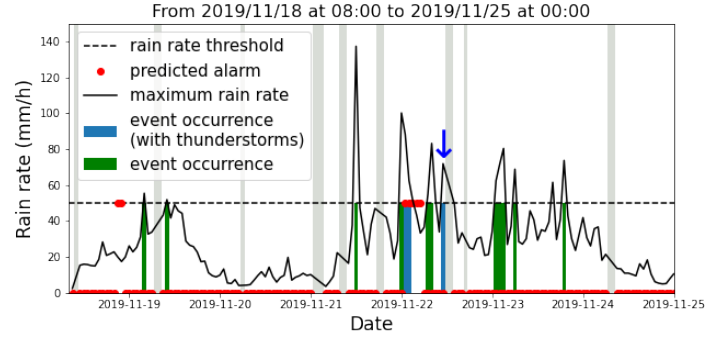
(c) TSS-ensemble ( $k = 10$ )

Figure 7: Predictions enrolled along time on the period of the test set obtained by applying the wTSS-ensemble strategy at  $k = 7$  run (top panel), the wTSS-ensemble strategy at  $k = 9$  run (central panel) and the TSS-ensemble strategy at  $k = 10$  run (bottom panel).

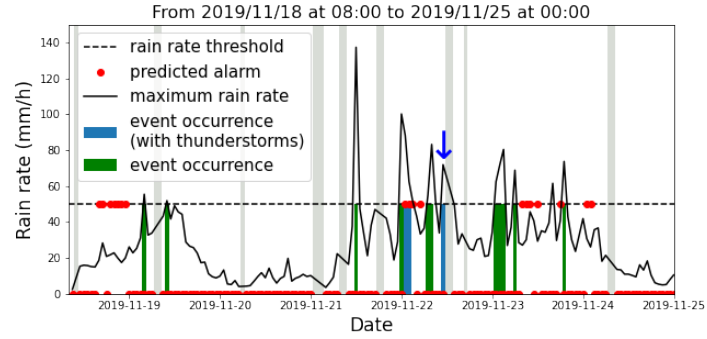
a skill score, as all the ones computed on a classical quality-based confusion matrix, does not account for the temporal distribution of alarms. Therefore, we propose to focus on value-weighted skill scores, as the wTSS, which account for the distribution of the predictions over time while promoting predictions in advance. We focused on the problem of forecasting extreme rainfall events on the Liguria region, and we showed that the performances of our ensemble technique in the case when wTSS is optimized, are significantly better than the performances of a standard quality-based score.



(a) wTSS-ensemble ( $k = 7$ )



(b) wTSS-ensemble ( $k = 9$ )



(c) TSS-ensemble ( $k = 10$ )

Figure 8: Predictions enrolled along time on the test period ranging from 2019/11/18 at 08:00 UTC to 2019/11/25 at 00:00 UTC obtained by applying the wTSS-ensemble strategy at  $k = 7$  run (top panel), the wTSS-ensemble strategy at  $k = 9$  run (central panel) and the TSS-ensemble strategy at  $k = 10$  run (bottom panel). The grey boxes correspond to time period where the input data are missing.

Next in line in our work will be the application of a class of score-driven loss functions [54], whose minimization in the training phase allows the automatic maximization of the corresponding skill scores. Further, we are currently investigating the impact of the use of more information, like the one involving number density and types of lightnings (such as cloud-to-cloud and cloud-to-ground strikes), on the prediction performances of the warning machine.

## Acknowledgment

SG is financially supported by a regional grant of the ‘Fondo Sociale Europeo’, Regione Liguria. MP and FB acknowledge the financial contribution from the agreement ASI-INAF n.2018-16-HH.0. We acknowledge the Italian Civil Protection Department, CIMA Research Foundation and the Italian Military Aeronautic for providing CAPPI radar data, MCM rainfall estimates and lightning data. We also acknowledge the support of a scientific agreement between ARPAL and the Dipartimento di Matematica, Università di Genova.

## References

- [1] S. Pensieri, M. E. Schiano, P. Picco, M. Tizzi, R. Bozzano, Analysis of the precipitation regime over the ligurian sea, *Water* 10 (5). doi:10.3390/w10050566.  
URL <https://www.mdpi.com/2073-4441/10/5/566>
- [2] D. Ricard, V. Ducrocq, V. Auger, A climatology of the mesoscale environment associated with heavily precipitating events over a Northwestern Mediterranean area, *J. Appl. Meteor. Climatol.* 51 (2012) 468–488.
- [3] U. Dayan, K. Nissen, U. Ulbrich, Review article: Atmospheric conditions inducing extreme precipitation over the eastern and western Mediterranean, *Natural Hazards and Earth System Sciences* 15 (11) (2015) 2525–2544.
- [4] F. Faccini, F. Luino, A. Sacchini, L. Turconi, Flash flood events and urban development in genoa (italy): lost in translation, in: *Engineering Geology for Society and Territory-Volume 5*, Springer, 2015, pp. 797–801.
- [5] F. Silvestro, S. Gabellani, F. Giannoni, A. Parodi, N. Rebora, R. Rudari, F. Siccardi, A hydrological analysis of the 4 November 2011 event in Genoa, *Nat. Hazards Earth Syst. Sci.* 12 (2012) 2743–2752.
- [6] A. Buzzi, S. Davolio, P. Malguzzi, O. Drofa, D. Mastrangelo, Heavy rainfall episodes over Liguria of autumn 2011: numerical forecasting experiments, *Nat. Hazards Earth Syst. Sci.* 14 (2014) 1325–1340.
- [7] E. Fiori, A. Commellas, L. Molini, N. Rebora, F. Siccardi, D. J. Gochis, S. Tanelli, A. Parodi, Analysis and hindcast simulation of an extreme rainfall event in the Mediterranean area: the Genoa 2011 case, *Atmos. Res.* 138 (2014) 13–29.

- [8] G. Delrieu, J. Nicol, E. Yates, P. E. Kirstetter, J.-D. Creutin, S. Anquetin, C. Obled, G.-M. Saulnier, V. Ducrocq, E. Gaume, O. Payrastre, H. Andrieu, P.-A. Ayrat, C. Bouvier, L. Neppel, M. Livet, M. Lang, J. P. du Châtelet, A. Walpersdorf, W. Wobrock, The catastrophic flash-flood event of 8-9 september 2002 in the Gard Region, France: A first case study for the Cévennes-Vivarais Mediterranean Hydrometeorological Observatory, *Natural Hazards and Earth System Sciences* 6 (1) (2005) 34–52.
- [9] N. Rebora, L. Molini, E. Casella, A. Commellas, E. Fiori, F. Pignone, F. Siccardi, F. Silvestro, S. Tanelli, A. Parodi, Extreme rainfall in the Mediterranean: what can we learn from observations?, *J. of Hydrometeorology* 14 (2013) 906–922.
- [10] F. Cassola, F. Ferrari, A. Mazzino, Numerical simulations of mediterranean heavy precipitation events with the wrf model: A verification exercise using different approaches, *Atmospheric Research* 164–165 (2015) 3–18.
- [11] F. Silvestro, N. Rebora, F. Giannoni, A. Cavallo, L. Ferraris, The flash flood of the Bisagno Creek on 9th October 2014: An “unfortunate” combination of spatial and temporal scales, *Journal of Hydrology* 541 (2016) 50 – 62, flash floods, hydro-geomorphic response and risk management. doi:<https://doi.org/10.1016/j.jhydrol.2015.08.004>.  
URL <http://www.sciencedirect.com/science/article/pii/S0022169415005636>
- [12] S. Davolio, F. Silvestro, T. Gastaldo, Impact of rainfall assimilation on high-resolution hydrometeorological forecasts over Liguria, Italy, *Journal of Hydrometeorology* 18 (10) (2017) 2659 – 2680.
- [13] E. Fiori, L. Ferraris, L. Molini, F. Siccardi, D. Kranzlmüller, A. Parodi, Triggering and evolution of a deep convective system in the Mediterranean Sea: modelling and observations at a very fine scale, *Quarterly Journal of the Royal Meteorological Society* 143 (703) (2017) 927–941. doi:<https://doi.org/10.1002/qj.2977>.
- [14] A. N. Meroni, A. Parodi, C. Pasquero, Role of sst patterns on surface wind modulation of a heavy midlatitude precipitation event, *Journal of Geophysical Research: Atmospheres* 123 (17) (2018) 9081–9096.
- [15] M. Lagasio, F. Silvestro, L. Campo, A. Parodi, Predictive capability of a high-resolution hydrometeorological forecasting framework coupling WRF cycling 3DVAR and continuum, *Journal of Hydrometeorology* 20 (7) (2019) 1307 – 1337. doi:[10.1175/JHM-D-18-0219.1](https://doi.org/10.1175/JHM-D-18-0219.1).
- [16] S. Davolio, F. Silvestro, P. Malguzzi, Effects of increasing horizontal resolution in a convection permitting model on flood forecasting: The 2011 dramatic events in Liguria (Italy), *J. Hydrometeor.* 16 (2015) 1843–1856.

- [17] F. Ferrari, F. Cassola, P. E. Tuju, A. Stocchino, P. Brotto, A. Mazzino, Impact of model resolution and initial/boundary conditions in forecasting flood-causing precipitations, *Atmosphere* 11 (2020) 592.
- [18] F. Cassola, F. Ferrari, A. Mazzino, M. M. Miglietta, The role of the sea on the flash floods events over Liguria (northwestern Italy), *Geophysical Research Letters* 43 (2016) 3534–3542.
- [19] F. Ferrari, F. Cassola, P. Tuju, A. Mazzino, Rans and les face to face for forecasting extreme precipitation events in the liguria region (northwestern italy), *Atmospheric Research* 259 (2021) 105654. doi:<https://doi.org/10.1016/j.atmosres.2021.105654>.  
URL <https://www.sciencedirect.com/science/article/pii/S0169809521002064>
- [20] S. Han, P. Coulibaly, Bayesian flood forecasting methods: A review, *Journal of Hydrology* 551 (2017) 340–351.
- [21] G. Blöschl, C. Reszler, J. Komma, A spatially distributed flash flood forecasting model, *Environmental Modelling & Software* 23 (4) (2008) 464–478.
- [22] A. Kauffeldt, F. Wetterhall, F. Pappenberger, P. Salamon, J. Thielen, Technical review of large-scale hydrological models for implementation in operational flood forecasting schemes on continental level, *Environmental Modelling & Software* 75 (2016) 68–76.
- [23] A. Hering, C. Morel, G. Galli, P. Ambrosetti, M. Boscacci, Nowcasting thunderstorms in the alpine region using a radar based adaptive thresholding scheme, in: *Proceedings, Third ERAD Conference, Visby, Sweden, 206-211, 2004*.
- [24] F. Silvestro, N. Rebora, Operational verification of a framework for the probabilistic nowcasting of river discharge in small and medium size basins, *Natural Hazards and Earth System Sciences* 12 (3) (2012) 763–776. doi:[10.5194/nhess-12-763-2012](https://doi.org/10.5194/nhess-12-763-2012).  
URL <https://nhess.copernicus.org/articles/12/763/2012/>
- [25] G. Ayzel, M. Heistermann, A. Sorokin, O. Nikitin, O. Lukyanova, All convolutional neural networks for radar-based precipitation nowcasting, *Procedia Computer Science* 150 (2019) 186–192, proceedings of the 13th International Symposium “Intelligent Systems 2018” (INTELS’18), 22-24 October, 2018, St. Petersburg, Russia. doi:<https://doi.org/10.1016/j.procs.2019.02.036>.  
URL <https://www.sciencedirect.com/science/article/pii/S1877050919303801>
- [26] G. Ayzel, T. Scheffer, M. Heistermann, Rainnet v1.0: a convolutional neural network for radar-based precipitation nowcasting, *Geoscientific Model Development* 13 (6) (2020) 2631–2644. doi:[10.5194/gmd-13-2631-2020](https://doi.org/10.5194/gmd-13-2631-2020).  
URL <https://gmd.copernicus.org/articles/13/2631/2020/>



- [27] S. Samsi, C. J. Mattioli, M. S. Veillette, Distributed deep learning for precipitation nowcasting, in: 2019 IEEE High Performance Extreme Computing Conference (HPEC), IEEE, 2019, pp. 1–7.
- [28] X. Shi, Z. Chen, H. Wang, D.-Y. Yeung, W.-k. Wong, W.-c. Woo, Convolutional lstm network: A machine learning approach for precipitation nowcasting, in: Proceedings of the 28th International Conference on Neural Information Processing Systems - Volume 1, NIPS’15, MIT Press, Cambridge, MA, USA, 2015, p. 802–810.
- [29] A. Heye, K. Venkatesan, J. E. Cain, Precipitation nowcasting : Leveraging deep recurrent convolutional neural networks, 2017.
- [30] Q.-K. Tran, S.-k. Song, Computer vision in precipitation nowcasting: Applying image quality assessment metrics for training deep neural networks, Atmosphere 10 (5). doi:10.3390/atmos10050244.  
URL <https://www.mdpi.com/2073-4433/10/5/244>
- [31] S. M. Bonnet, A. Evsukoff, C. A. Morales Rodriguez, Precipitation nowcasting with weather radar images and deep learning in são paulo, brasil, Atmosphere 11 (11). doi:10.3390/atmos11111157.  
URL <https://www.mdpi.com/2073-4433/11/11/1157>
- [32] G. Czibula, A. Mihai, E. Mihuleț, Nowdeepn: An ensemble of deep learning models for weather nowcasting based on radar products’ values prediction, Applied Sciences 11 (1). doi:10.3390/app11010125.  
URL <https://www.mdpi.com/2076-3417/11/1/125>
- [33] X. Shi, Z. Gao, L. Lausen, H. Wang, D.-Y. Yeung, W.-k. Wong, W.-c. WOO, Deep learning for precipitation nowcasting: A benchmark and a new model, in: I. Guyon, U. V. Luxburg, S. Bengio, H. Wallach, R. Fergus, S. Vishwanathan, R. Garnett (Eds.), Advances in Neural Information Processing Systems, Vol. 30, Curran Associates, Inc., 2017.  
URL <https://proceedings.neurips.cc/paper/2017/file/a6db4ed04f1621a119799fd3d7545d3d-Paper.pdf>
- [34] G. Franch, D. Nerini, M. Pendesini, L. Coviello, G. Jurman, C. Furlanello, Precipitation nowcasting with orographic enhanced stacked generalization: Improving deep learning predictions on extreme events, Atmosphere 11 (3). doi:10.3390/atmos11030267.  
URL <https://www.mdpi.com/2073-4433/11/3/267>
- [35] M. L. Poletti, F. Silvestro, S. Davolio, F. Pignone, N. Rebora, Using nowcasting technique and data assimilation in a meteorological model to improve very short range hydrological forecasts, Hydrology and Earth System Sciences 23 (9) (2019) 3823–3841. doi:10.5194/hess-23-3823-2019.  
URL <https://hess.copernicus.org/articles/23/3823/2019/>

- [36] X.-H. Le, H. V. Ho, G. Lee, S. Jung, Application of long short-term memory (lstm) neural network for flood forecasting, *Water* 11 (7) (2019) 1387.
- [37] G. Van Houdt, C. Mosquera, G. Nápoles, A review on the long short-term memory model., *Artif. Intell. Rev.* 53 (8) (2020) 5929–5955.
- [38] J. Donahue, L. Hendricks, M. Rohrbach, S. Venugopalan, S. Guadarrama, K. Saenko, T. Darrell, Long-term recurrent convolutional networks for visual recognition and description. retrieved 30 august 2019 (2019).
- [39] S. Guastavino, M. Piana, F. Benvenuto, Bad and good errors: value-weighted skill scores in deep ensemble learning, *arXiv preprint arXiv:2103.02881*.
- [40] D. Atlas, *Radar in Meteorology: Battan Memorial and 40th Anniversary Radar Meteorology Conference*, Springer, 2015.
- [41] G. Bruno, F. Pignone, F. Silvestro, S. Gabellani, F. Schiavi, N. Rebora, P. Giordano, M. Falzacappa, Performing hydrological monitoring at a national scale by exploiting rain-gauge and radar networks: The italian case, *Atmosphere* 12 (6). doi:10.3390/atmos12060771.  
URL <https://www.mdpi.com/2073-4433/12/6/771>
- [42] D. Biron, Lampinet–lightning detection in italy, in: *Lightning: Principles, Instruments and Applications*, Springer, 2009, pp. 141–159.
- [43] J. Donahue, L. A. Hendricks, M. Rohrbach, S. Venugopalan, S. Guadarrama, K. Saenko, T. Darrell, Long-term recurrent convolutional networks for visual recognition and description, *IEEE Transactions on Pattern Analysis and Machine Intelligence* 39 (4) (2017) 677–691. doi:10.1109/TPAMI.2016.2599174.
- [44] I. Goodfellow, Y. Bengio, A. Courville, *Deep learning*, MIT press, 2016.
- [45] X. Glorot, Y. Bengio, Understanding the difficulty of training deep feedforward neural networks, in: Y. W. Teh, M. Titterton (Eds.), *Proceedings of the Thirteenth International Conference on Artificial Intelligence and Statistics*, Vol. 9 of *Proceedings of Machine Learning Research*, PMLR, Chia Laguna Resort, Sardinia, Italy, 2010, pp. 249–256.  
URL <http://proceedings.mlr.press/v9/glorot10a.html>
- [46] F. Chollet, *Keras* (2015).  
URL <https://github.com/fchollet/keras>
- [47] N. Srivastava, G. Hinton, A. Krizhevsky, I. Sutskever, R. Salakhutdinov, Dropout: a simple way to prevent neural networks from overfitting, *The journal of machine learning research* 15 (1) (2014) 1929–1958.
- [48] D. S. Bloomfield, P. A. Higgins, R. J. McAteer, P. T. Gallagher, Toward reliable benchmarking of solar flare forecasting methods, *The Astrophysical Journal Letters* 747 (2) (2012) L41.

- [49] D. P. Kingma, J. Ba, Adam: A method for stochastic optimization, Proceedings of 3rd International Conference on Learning Representations.
- [50] M.-J. Chang, H.-K. Chang, Y.-C. Chen, G.-F. Lin, P.-A. Chen, J.-S. Lai, Y.-C. Tan, A support vector machine forecasting model for typhoon flood inundation mapping and early flood warning systems, *Water* 10 (12) (2018) 1734.
- [51] F. Benvenuto, C. Campi, A. M. Massone, M. Piana, Machine learning as a flaring storm warning machine: Was a warning machine for the 2017 september solar flaring storm possible?, *The Astrophysical Journal Letters* 904 (1) (2020) L7.
- [52] Z. Zhang, Y. Chen, Tail risk early warning system for capital markets based on machine learning algorithms, *Computational Economics* (2021) 1–23.
- [53] H. Li, C. Li, Y. Liu, Machine learning-based frequency security early warning considering uncertainty of renewable generation, *International Journal of Electrical Power & Energy Systems* 134 (2022) 107403.
- [54] F. Marchetti, S. Guastavino, M. Piana, C. Campi, Score-oriented loss (sol) functions, arXiv preprint arXiv:2103.15522.